Experimental evaluation of the air trapped during the water entry of flexible structures

Riccardo Panciroli[1], Giangiacomo Minak[2]

[1] *Università degli studi Niccolò Cusano. Via Don Carlo Gnocchi, 3. 00166 Roma, Italy*
[2] *DIN – Alma Mater Studiorum. Viale del Risorgimento, 2. 40136 Bologna, Italy*

ABSTRACT
Deformable structures entering the water might experience several fluid-structure interaction (FSI) phenomena; air trapping is one of these. According to its definition, it consists of air bubbles trapped between the structure and the fluid during the initial stage of the impact. These bubbles might reduce the peak impact force. This phenomenon is characteristic for the water entry of flat-bottom structures. Above a deadrise angle of 10°, air trapping is negligible. In this work, we propose a methodology to evaluate the amount of air trapped in the fluid during the water entry. Experiments are performed on wedges with varying stiffness, entry velocity, and deadrise angle. A digital image post-processing technique is developed and utilized to track the air trapping mechanism and its evolution in time. Interesting results are found on the effect of the impact velocity and the structural deformation on the amount of air trapped during the slamming event.

1. INTRODUCTION

Predicting the impact-induced stresses during the water entry of flexible structures is of major interest for the design of marine structures. During the water entry of flexible structures, several fluid structure interaction (FSI) phenomena might appear [1]–[9]. The most important are: cavitation, air trapping, and repetition of impact and separation between the fluid and the structure. The occurrence of such FSI phenomena might strongly influence the impact dynamics.

Although air trapping is a well-known phenomenon [10], to the author's knowledge none of the previous works in the literature presented a methodology to quantify it and evaluate the effect of the structural deformation on it. The present work faces this challenge, proposing the use of an optical technique to achieve this aim. Optical techniques have been recently utilized to measure the structural deformation of compliant wedges entering the water in [11].

In this work, we firstly develop a digital imaging technique for the post-processing of high-speed images to isolate the regions of the fluid where air is trapped. This methodology is later used to study the evolution of the air trapping in time and to dissect the role of impact velocity and structural deformation.

Although there are no previous results in the literature to validate the proposed method, the present results are found in good agreement with the expectations.

2. EXPERIMENTAL SETUP

Experiments are conducted on a drop weight machine for water impacts with a maximum impact height of 4 m. Wedges are comprised by two panels joined together and to the falling sledge on one edge to assume a cantilever boundary condition, where the boundary corresponds to the keel of the wedge. Panels of various material and thickness can be mounted on the
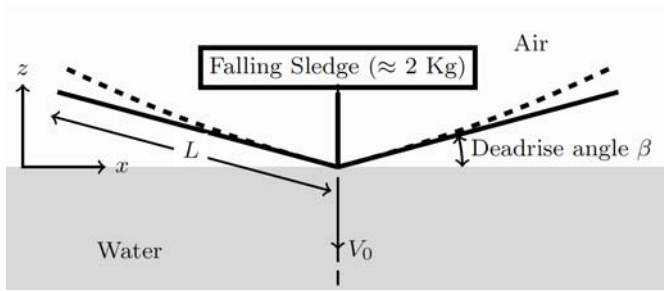
Figure 1. Conceptual scheme of the wedge used for experiments. L = panel length. β = deadrise angle. Solid line: undeformed panels, dashed line: expected deformation during impact.

Figure 3. Sample of an image captured by the high-speed camera. The still water above the transparent screen is clearly visible. The lighter dots clearly visible in the fluid are air bubbles that are used as tracers in the PIV analysis.

sledge at any deadrise angle (β in Figure 1) ranging smoothly from 0° to 50°, where 0° and 90° are the extreme case of a flat panel and a vertical blade, respectively.

Teflon insets minimize friction between the sledge and the prismatic rails. The sledge holds wedges 300 mm long and 250 mm wide. The falling body hits the fluid at the centre of a tank 1.2 meters wide, 1.8 meters long and 1.1 m deep. The tank was filled with water only up to 0.6 m to prevent the water waves generated during the impact to overflow. The drop height, defined as the distance between the keel and the water surface, ranged from 0.5 m to 3 m at 0.25 m increments. Impact acceleration is measured by a V-Link Microstrain wireless accelerometer (±100g) located at the tip of the wedge. All reported accelerations are referenced to 0 g for the free-falling phase. The sampling frequency is set to its maximum of 4 kHz. Entering velocity is recorded by a laser sensor ($\mu\varepsilon$ ILS 1402) capturing the sledge position over 350 mm of ride at a frequency of 1.5 kHz with a definition of 0.2 mm. The entry velocity is obtained by the numerical differentiation of the position.

A high-speed camera is utilized to capture the images during the water entry. The camera is located to view the wedge from the side, as shown in Figure 2. The capturing frequency is set to 1.5 kHz with a definition of 1200×1024 pixels. A vertical transparent screen is located inside the water tank just before the wedge (clearance is ≈2 mm) to prevent fluid spray in the y-direction, which would have made it impossible to see the evolution of the fluid jet (Figure 3) generated during the water entry. As the water on the front side of the screen remains still during the impact, pictures show both the still water surface (on the front side of the screen) and the fluid jet (on the back side
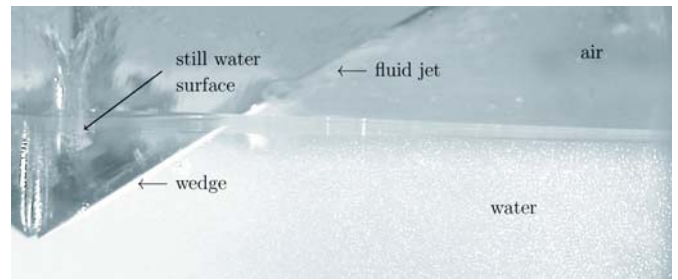
of the screen), as shown in Figure 3.

Aluminium (A), E-glass (mat) / vinyl ester (V) and E-Glass (woven) / epoxy (W) panels 2 mm thick were used.

Composite panels were produced by VARTM by infusion of vinyl ester resin on E-Glass fibre mat, while the E-glass (woven 0°/90°) / epoxy panels were produced in an autoclave. The assumed material properties and the measured fundamental frequency of the panels are listed in Table 1.

For given material and panels thickness, the impact variables are: deadrise angle β (range 4° to 35°) and falling height (ranging 0.25 to 2.5 m). During the experiments, structural deformations are recorded by strain gauges located at various positions, while an accelerometer and a laser position sensor record the impact dynamics. The wedges are built as an open-structure, as the sides of the panels are open and the water is free to flow from the sides during impact (this setup is necessary to allow higher flexibility). This leads the entire structure to be theoretically negatively buoyant. However, the impact time is very short, as it typically lasts less than 40 ms (the structure enters the water with an entry velocity in the range of 4 to 6 m/s). In such a short duration, the water has not enough time to flow into the wedge from the sides, so it behaves like a closed-shape wedge, with a positively buoyant behaviour (the acceleration range is approximately 20 g to 100 g, increasing with the entry speed).

Wedges are manually lifted to the desired height and released. Laser sensor, strain gauges, and accelerometer signals are triggered together in a single manual start. Since the position of the sledge relative to the free surface is known, the initial impact time is calibrated during the data post-processing on the basis of the position recorded by the laser sensor.

3. PRELIMINARY EXPERIMENTAL RESULTS

In the following, we display some images captured during the water entry of wedges with deadrise angles higher than 10°. The examples evaluate the air trapped for variable (high to low) deadrise angle. Two impact velocities are shown for each deadrise angle.

Figure 4 shows the water entry of a wedge with deadrise angle of 30° entering the water at 4.2 m/s and 6 m/s. In both cases no water is trapped in the fluid, as indicated by the smooth uniform colour in the fluid region.
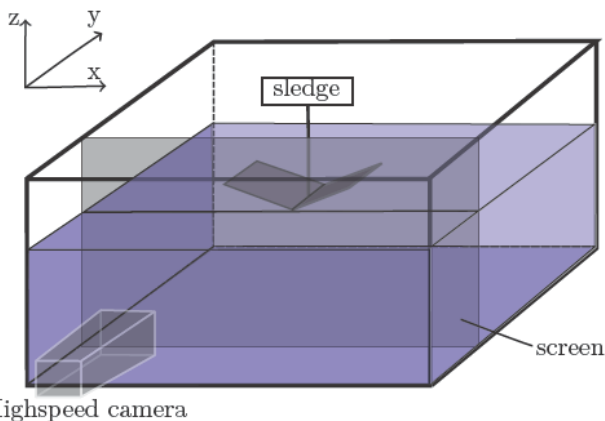

Figure 2. Sketch of the experimental set-up. The wedge is hinged to the sledge that enters the water with pure vertical velocity. The high-speed camera is located on the side of the water tank.

Table 1. Collection of the estimated material properties.

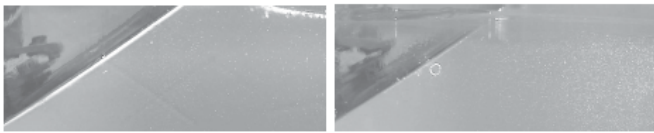| Material	$E_1=E_2$ [GPa]	ν	ρ [kg/m^3]	ω_n [Hz]
6068 T6	68	0.32	2700	18.01
E-Glass/vinylester	20.4	0.28	2050	9.77
E-Glass /epoxy	30.3	0.28	2015	19.69

Figure 4. Image of a wedge with deadrise angle of 30° entering the water at 4.2 m/s (left) and 6 m/s (right). The fluid shows a uniform colour, meaning that no air has been trapped during the water entry.

Figure 5. Image of a wedge with deadrise angle of 20° entering the water at 4.2 m/s (left) and 6 m/s (right). There is no air trapped in the case of lower entry velocity while some very small air bubbles appear in the case of larger velocity.

Figure 6. Image of a wedge with deadrise angle of 15° entering the water at 4.2 m/s (left) and 6.7 m/s (right). In both cases there is some air trapped in the fluid in the form of small air bubbles.

Figure 7. Image of a wedge with deadrise angle of 12° entering the water at 5.2 m/s (left) and 6.7 m/s (right). Air trapping is much more visible than the previous cases since a concentrated light is used to highlight the air bubbles.

Figure 5 shows the water entry of a wedge with deadrise angle of 20° entering the water at 4.2 m/s and 6 m/s. While in the first image there is no evidence of air trapped in the fluid, the wedge impacting at higher speed (picture on the right) is trapping some air in the form of small bubbles that appear at the middle of the wedge. Although existing, air trapping is still negligible for this deadrise angle.

Wedges with deadrise angle of 15° (shown in Figure 6) show results similar to the last example. Even for this deadrise angle some negligible air bubbles are trapped in the fluid.

Air bubbles are definitely spread on a wider region in the case of a deadrise angle of 12°, as shown in Figure 7.

Until the deadrise angle of 12° no air cushions are formed: air is trapped in the form of small bubbles dispersed in the fluid and its effect can be neglected. Instead, air cushions are formed for deadrise angles lower than 12°, indicating that our results are in line with the literature.

In the following sections, the research will focus on the water entry of wedges with deadrise angle lower than 12° with particular effort on evaluating the amount of air trapped in the fluid, its evolution in time, and the effect of the structural deformation on it. As the first step, a digital image post-processing methodology capable of evaluating the amount of air trapped in the fluid has been developed and is presented in the next section.
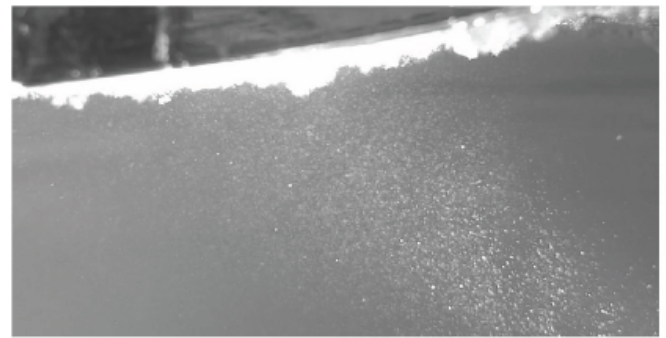

Figure 8. Example of an image where some air is trapped in the fluid during the impact. Air appears as a bright region due to the light that is diffracted by the surface of the air bubbles.

4. THE USE OF AN OPTICAL METHOD TO ACCOUNT FOR THE AIR TRAPPED DURING THE WATER ENTRY

To track the evolution of the air trapped during the water entry, a digital image technique has been developed to post–process the high-speed images. This technique relies on the properties of the water surface to diffract the light: as air bubbles are entrapped in the fluid, if lightened by a light source, their surface will diffract the light making them brighter than the surrounding fluid.

Images with a definition of 1200×1024 pixels are captured by the camera at a rate of 1.5 kHz. An example of a typical image where air is trapped into the fluid is shown in Figure 8.

Images (originally in colour) are converted to greyscale, that is, images are represented by a matrix where the cells assume a value between 0 and 255, where 0 corresponds to a fully black pixel and 255 to a fully white pixel. All the values in between define the grey level. The intensity of the grey levels vs. the pixels counts are plotted as a histogram (Figure 9).

We choose for the relation between the magnitude of air trapped below the structure and the number of pixels exceeding a certain grey level. Each pixel corresponds to an area of 0.23×0.23 mm², since the calibration gave that 1305 pixels correspond to 300 mm in length.

Upon an independent study on the role of the threshold level on the evaluated results on the computed amount of trapped air, we choose 200 as the threshold level above which the pixels have to be considered air. Such threshold level was found to be extremely affected by the lighting parameters used during the image acquisition: diaphragm aperture and exposition time (inversely proportional to the capturing
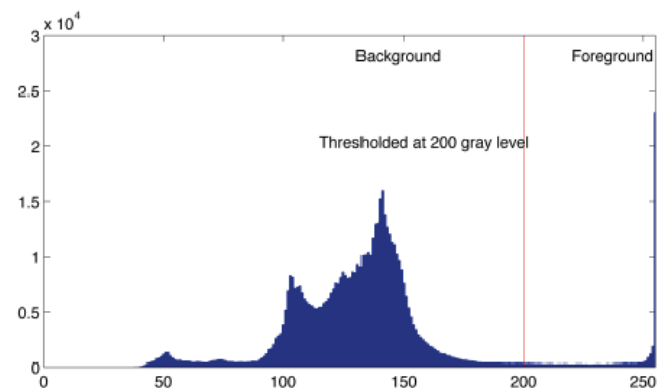

Figure 9. Example of a histogram of the grey level (0 to 256) vs. pixel count of the greyscale image.

frequency). However, we comment that, for a given diaphragm aperture and exposition time, variations of the threshold level from the reference value by 20% have negligible effects on the results.

A new binary image is then built: pixels below the threshold are set as black (0), while pixels exceeding the threshold are set as white (255). A black and white picture is obtained this way. To smooth out the images and clear possible lonely black pixels isolated in wide white regions an algorithm based on morphological reconstruction described in [12] is applied to the images. Later, the general procedure outlined in [13] is applied to compute the white regions. As output, the white regions are listed and their perimeter and area is reported. Small air bubbles are dispersed in the water even before the impact. A threshold on the minimum size of the area is thus used to neglect these small bubbles from the evaluation of the total amount of air trapped during the water entry. The number of white regions is thus filtered to exclude those with an area smaller than 12 pixels, as this value has been evaluated to correspond to the area of the air bubbles already trapped in the fluid before the impact. The total area of air trapped below the structure is thus evaluated as it is assumed to be proportional to the number of pixels counted with the proposed method.

5. ON THE EFFECT OF THE ENTRY VELOCITY ON THE TRAPPED AIR

This section investigates the effect of the entry velocity on the amount of air trapped during the initial stage of the impact.

Using the technique presented in the previous section, it is possible to observe the time trace of the trapped air. The analysis is performed on wedges with deadrise angle of 4° entering the water in free fall from several impact heights: namely 50, 100, 150, and 200 cm. Wedges are all 2 mm thick and are made by three different materials: Aluminium, Woven-glass/epoxy and matt E-glass/vinyl ester. This way the impact conditions were similar but bodies presented different flexibility due to the differences in the elasticity modulus of the three materials (namely 68 GPa, 30.3 GPa and 20.2 GPa). A detailed characterization of the specimens can be found in [14]. It was thus possible to study the effect of the structural deformation on the air trapped during the impact.

Figures 10 to 12 show the results of the evaluated trapped air versus the entry depth $V_0 t$, where V_0 is the velocity at the beginning of the impact.
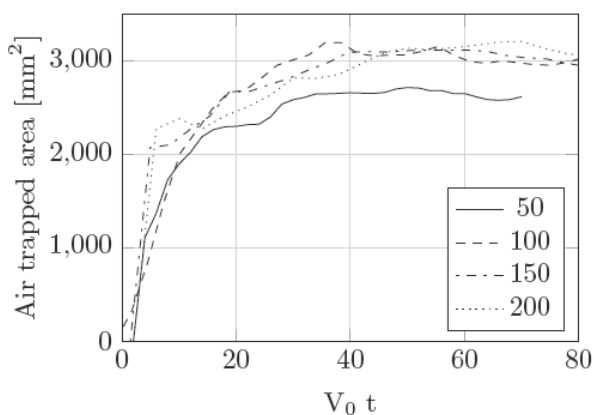

Figure 10. Experimental evaluation of the air trapped in time. Aluminium wedge (A) 2 mm thick, deadrise angle $\beta = 4°$, for variable impact height. The impact heights in the legend are in cm. The product $V_0 t$ is in mm.

Figure 11. Experimental evaluation of the air trapped in time. Composite wedge (W) 2 mm thick, deadrise angle $\beta = 4°$, for variable impact height. The impact heights in the legend are in cm. The product $V_0 t$ is in mm.

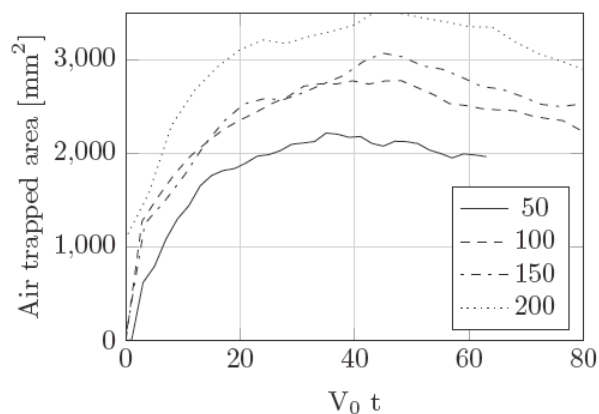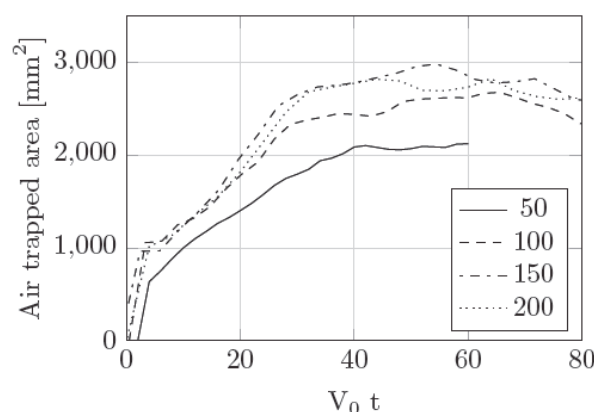Figure 12. Experimental evaluation of the air trapped in time. Composite wedge (V) 2 mm thick, deadrise angle $\beta = 4°$, for variable impact heights. The impact heights in the legend are in cm. The product $V_0 t$ is in mm.

6. EFFECT OF THE STRUCTURAL DEFORMATION ON THE AIR TRAPPED DURING THE WATER ENTRY

In the case of the water entry of flexible structures, there is the possibility that the structural deformation alters the air trapping mechanism. In particular, considering simple wedges, the deadrise angle is locally modified during the impact with water and this could lead air bubbles to coalesce and to form a cushion, or, on the other side, it could let the air escape from an already present cushion. An example of wedge deflection evolution during the water impact can be found in [8].

A collection of the experimental results for the different wedges impacting from the same heights is presented in Figure 13. The experimental findings suggest that the flexibility of the wedge has negligible effects on the air trapping, as wedges assume large deformations once the air has been already entrapped in the fluid. Even if the amount of trapped air is quite similar in all the three cases, it may be noted that, at the beginning of the water entry, stiffer wedges show a sharper peak of entrapped air, for high impact energies, than the more flexible ones. Instead, the more flexible wedges apparently loose some air from the cushions in the final part of the entry. Further investigation is needed to further explore and confirm such findings.
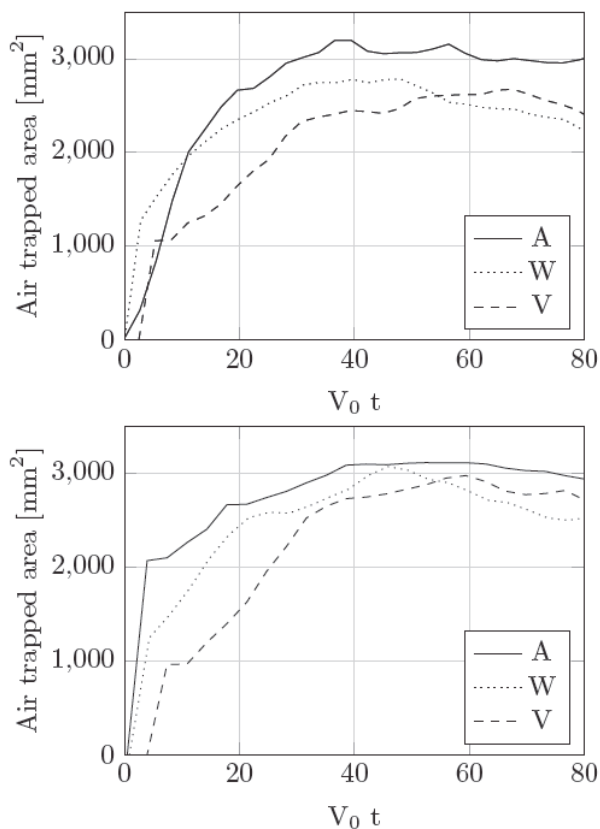
Figure 13. Evolution of the air entrapped in time for the water entry of wedges with various flexural stiffness (A=Aluminium, W=Woven Glass/Epoxy, V= Mat Glass/Epoxy) impacting from two different impact heights (100 cm - Top, and 150 cm – Bottom). The product $V_0 t$ is in mm.

7. CONCLUSIONS

In this work we propose a technique to quantify the amount and the evolution in time of the air trapped during the water entry of flexible structures. First, a methodology based on the analysis of the high-speed images is proposed and commented. Results are found to be in agreement with the expectations, although only qualitative comparison can be done, as there are no other experimental, nor numerical results in the literature to compare our results with.

On the base of the experimental findings, air trapping seems to attain its maximum at the beginning of the impact, when the velocities are higher. However, bodies need time to deform: when the wedge deformations are large enough to modify the deadrise angle, the entireness of the entrapped air has been already trapped in the fluid. On the basis of these preliminary results, there is no experimental remarkable evidence of the influence of the structural deformation on the amount of air trapped during the impact. Further studies are needed to confirm this observations.

The analysis of the images showed that wedges with deadrise angles greater than 10° entrap the air in the form of small bubbles spread on a region that decreases as the deadrise angle increases. In the cases investigated, the structural deformation was not capable of lowering the deadrise angle enough to switch the air trapping mechanism from small air bubbles (with negligible effect on the hydrodynamic pressure) to an air cushion, which might have a strong effect on the hydrodynamic pressure. Indeed, further investigations in this direction are needed to deeply understand this phenomenon.

The experimental results show a saturating effect of the impact energy on the amount of entrapped air. Furthermore, the role of the stiffness is very limited, as air trapping is found to mainly relate to the initial deadrise angle. Further investigations are needed for the cases with very low deadrise angles and different geometries.

We comment that the recently developed methodologies to reconstruct the hydrodynamic pressure in water entry problems from the flow kinematic components [15-17] can be adopted in the future to quantify the influence of air trapping on the hydrodynamic pressure.

REFERENCES

[1] S. Abrate, Hull slamming, Appl. Mech. Rev. 64 (2013) p.060803.
[2] A. Korobkin, E.I. Părău, J.M. Vanden-Broeck, The mathematical challenges and modelling of hydroelasticity, Philos. Trans. A. Math. Phys. Eng. Sci. 369 (2011) pp. 2803-2812.
[3] S.E. Hirdaris, P. Temarel, Hydroelasticity of ships: recent advances and future trends, Proc. Inst. Mech. Eng. Part M J. Eng. Marit. Environ. 223 (2009) pp. 305–330.
[4] X. Chen, Y. Wu, W. Cui J.J. Jensen, Review of hydroelasticity theories for global response of marine structures, Ocean Eng. 33 (2006) pp. 439–457.
[5] O.M. Faltinsen, The effect of hydroelasticity on ship slamming, Philos. Trans. R. Soc. A Math. Phys. Eng. Sci. 355 (1997) pp. 575–591.
[6] O.M. Faltinsen, Hydroelastic slamming, J. Mar. Sci. Technol. 5 (2000) pp. 49–65.
[7] R. Panciroli, Water entry of flexible wedges : Some issues on the FSI phenomena, Appl. Ocean Res. 39 (2012) pp. 72–74.
[8] R. Panciroli, S. Abrate, G. Minak, A. Zucchelli, Hydroelasticity in water-entry problems: Comparison between experimental and SPH results," Compos. Struct. 94 (2012) pp. 532–539.
[9] R. Panciroli, S. Abrate, G. Minak, Dynamic response of flexible wedges entering the water, Compos. Struct., 99 (2013) pp. 163-171.
[10] A. Korobkin, A.S. Ellis, F.T. Smith, Trapping of air in impact between a body and shallow water, J. Fluid Mech. 611 (2008) pp. 365–394.
[11] M. Cooper, L. McCue, "Experimental study on deformation of flexible wedge upon water entry," in 9th Symposium on High Speed Marine Vehicles.
[12] P. Soille, Morphological Image Analysis: Principles and Applications. Springer-Verlag, 1999, pp. 173–174.
[13] R.M. Haralick, L.G. Shapiro, Computer and Robot Vision, 1st ed. Boston, MA, USA: Addison-Wesley Longman Publishing Co., Inc., 1992.
[14] R. Panciroli, Dynamic Failure of Composite and Sandwich Structures, vol. 192. Dordrecht: Springer Netherlands, 2013.
[15] A. Nila, S. Vanlanduit, S. Vepa, W. Van Paepegem, A PIV-based method for estimating slamming loads during water entry of rigid bodies, Meas. Sci. Technol., 24 (2013) p. 045303.
[16] B.W. van Oudheusden, PIV-based pressure measurement, Meas. Sci. Technol., 24 (2013) p. 032001.
[17] R. Panciroli, M. Porfiri, Evaluation of the pressure field on a rigid body entering a quiescent fluid through particle image velocimetry, Exp. Fluids 54 (2013) p. 1630.